 MCB, vol.15, no.2, pp.99-115, 2018

# Combining Smaller Patch, RV Remodeling and Tissue Regeneration in Pulmonary Valve Replacement Surgery Design May Lead to Better Post-Surgery RV Cardiac Function for Patients with Tetralogy of Fallot

**Zhedian Zhou[1], Tal Geva[2], Rahul H. Rathod[2], Alexander Tang[2], Chun Yang[3], Kristen L. Billiar[4], Dalin Tang[1, *, 3] and Pedro del Nido[5]**

**Abstract:** Patients with repaired Tetralogy of Fallot (ToF), a congenital heart defect which includes a ventricular septal defect and severe right ventricular outflow obstruction, account for the majority of cases with late onset right ventricle (RV) failure. The current surgical approach, which includes pulmonary valve replacement/insertion (PVR), has yielded mixed results. A computational parametric study using 7 patient-specific RV/LV models based on cardiac magnetic resonance (CMR) data as "virtual surgery" was performed to investigate the impact of patch size, RV remodeling and tissue regeneration in PVR surgery design on RV cardiac functions. Two patch sizes, three degrees of scar trimming (RV volume shrinkages: 9%, 17%, 25%) and hypothetical use of regenerated myocardium as replacement of patch and scar were considered in these models. Our preliminary results indicate that each of the three techniques (smaller patch, RV remodeling, and myocardium regeneration) had modest improvement on post-PVR RV ejection fraction (from 1.76%-4% over the conventional PVR procedure) and combination of all three techniques had the best performance (a 4.74% improvement in ejection fraction over the conventional PVR, for the patient studied). Changes in RV stress, strain and curvatures were also observed. However, their linkages to RV ejection fraction were less clear. Further investigations are required to confirm our findings.

**Keywords:** Heart modeling, cardiac mechanics, right ventricle, tetralogy of Fallot, virtual surgery.

[1] School of Biological Science & Medical Engineering, Southeast University, Nanjing, 210096, China.

[2] Department of Cardiology, Boston Children's Hospital, Department of Pediatrics, Harvard Medical School, Boston, MA 02115 USA.

[3] Mathematical Sciences Department, Worcester Polytechnic Institute, Worcester, MA 01609, USA.

[4] Department of Biomedical Engineering, Worcester Polytechnic Institute, MA 01609, USA.

[5] Department of Cardiac Surgery, Boston Children's Hospital, Department of Surgery, Harvard Medical School, Boston, MA 02115 USA

* Corresponding author: Dalin Tang. Email: dtang@wpi.edu.

## 1 Introduction

Right ventricular (RV) dysfunction is a common cause of heart failure in patients with congenital heart defects and often leads to impaired functional capacity and premature death [del Nido (2006)]. Patients with repaired Tetralogy of Fallot (TOF), a congenital heart defect which includes a ventricular septal defect and severe right ventricular outflow obstruction, account for the majority of cases with late onset RV failure. The current surgical approach, which includes pulmonary valve replacement/insertion (PVR), has yielded mixed results [Therrien, Siu, Mclaughlin et al. (2000); Vliegen, Van, De et al. (2002); Waien, Liu, Ross et al. (1992)]. Dr. del Nido and Dr. Geva et al. reckoned that the reason for the unpredictable results is the fact that the PVR surgery only addresses one mechanism for RV dysfunction and dilatation, namely pulmonary regurgitation. They proposed a novel surgical procedure to improve post-PVR outcome, which included use of smaller patch and more radical removal of scar tissue [del Nido (2006)] (see Fig. 1). In this paper, we took a computational approach and performed parametric analysis using 7 patient-specific RV/LV models as "virtual surgery" to investigate the impact of patch size, RV remodeling and tissue regeneration in PVR surgery design on right ventricle cardiac functions.

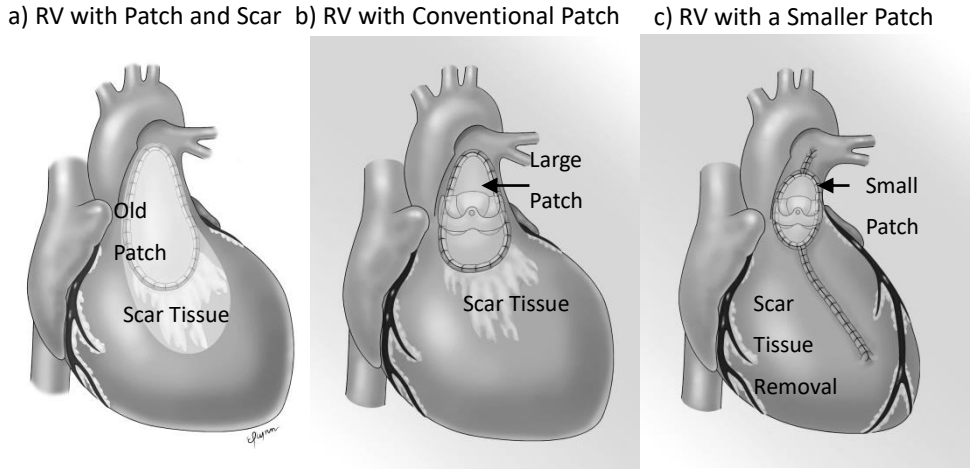


**Figure 1:** Illustration of PVR surgical options for TOF patients. (a) A diseased RV with old patch and scar tissue; b) RV after PVR surgery, conventional patch; c) RV after PVR with scar removal and a smaller patch

Image-based computational modeling and medical imaging technologies have made considerable advances in biological and clinical research in recent years [Geva, Powell, Crawford et al. (1998); Geva, Greil, Marshall et al. (2002); Geva, Sandweiss, Gauvreau et al. **(**2004); Haber (2000); Tang, Yang, Geva et al. (2007, 2010); Tang, del Nido, Yang et al. (2016); Axel (2002)]. These efforts have made it possible to introduce computer-simulated procedures into clinical decision-making process instead of empirical and often risky clinical experimentation to examine the efficiency and suitability of various reconstructive procedures and patch design in diseased hearts [Yang, Tang, Haber et al. (2007); Tang, Yang, Geva et al. (2007, 2008); McCulloch, Waldman, Rogers et al.

(1992,2007); Saber Gosman, Wood et al. (2001); Wenk, Zhang, Cheng et al. (2010); Guccione and Mcculloch (1993); Guccione, Costa and Mcculloch (1995); Guccione, Le, de Tombe et al. (1997); Long, Merrifield, Yang et al. (2003); Long, Merrifield, Xu et al. (2008); Vetter and McCulloch (2000); Ghista, Zhong, Chua et al. (2005)]. In recent years, we have introduced patient-specific RV/LV models with and without fluid-structure interactions for TOF patients to identify possible risk factors which could be used to differentiate patients with better outcome from patients with worse outcome [Tang, Yang, Geva et al. (2007, 2014); Tang, del Nido, Yang et al. (2016); Tang, Zuo, Wu et al. (2017)]. Our preliminary results indicated that RV stress was the only factor which showed significant difference between the better-outcome group (n=8) and worse-outcome group (n=8) [Tang, del Nido, Yang et al. (2016); Tang, Zuo, Wu et al. (2017)]. In another paper, they also presented some preliminary results showing that mean longitudinal curvature (L-cur) from better-outcome group was 36.5% higher than that from the worse-outcome group [Tang, Yang, Geva et al. (2014)]. Those preliminary results were based on limited number of patients and require further investigation and validations.

In this paper, a pre-operative RV/LV model and 6 virtual surgery models were constructed to investigate the effects of patch size, scar tissue trimming and scarred myocardium repair on RV cardiac function and mechanical performances. Our models included (a) RV intraventricular pressure data; (b) two-layer ventricle wall construction with realistic epicardium and endocardium fiber orientations; (c) anisotropic material properties; (d) a structure-only LV as support to the RV structure; (e) different degrees of scar tissue trimming, small or large patch, normal or ideal patch material and tissue engineering for scarred myocardial tissue regeneration. Details of the pre-operative and virtual surgery models are given below.

## 2 Methods and models

### *2.1 Data acquisition*

Cardiac MRI data were acquired and analyses were performed by Dr. Tal Geva at Children's Hospital Boston for the patients needing RV remodeling and PVR operations with written consent obtained. Data acquisition and analysis procedures were previously published and details are omitted here [Tang, Yang, Geva et al. (2010, 2013); Yang, Tang, Geva et al. (2013)]. Some key features of the data are provided here for easy reading. Electrocardiography-gated steady state free precession cine MRI was used to image the patients' hearts and acquire the patient-specific ventricle geometry data. 11-14 equidistant slices were obtained in the ventricular short-axis plane covering both left and right ventricle from the atrioventricular junction to apex (slice thickness 6-8 mm; interslice gap 0-2 mm; 30 frames during one cardiac cycle). MRI data from one patient (male, 47 years old) was used in this paper to construct models simulating various surgical PVR options for better post-PVR outcome. For this data set, slice thickness is 8 mm; interslice gap is 2 mm; cardiac cycle is 0.82 s. The position and sizes of the patch and scar tissues were determined by Dr. delNido based on his 20-years surgical experience and intraoperative observation. Image Segmentation and other further analysis were performed by a commercially available software package for quantitative analysis of cardiac MRI studies (QMass, Medis

Medical Imaging Systems, Leiden, the Netherlands) to get blood-endocardium boundaries and epicardial borders. Fig. 2 gave selected MRI slices, segmented slice contour plots, stacked contour 3D view, and 3D plots showing patch, scar and pulmonary outflow track. Simpson's method was used to calculate end-diastolic volume (EDV), end-systolic volume (ESV), ejection fraction (EF), stroke volume (SV), ventricular mass, and mass-to-volume ratio.

Since patient-specific fiber orientation data and anisotropic material properties are not available with the current technology, fiber orientation angles were assigned to every finite element using data from available literature [Hunter, Pullan and Smaill (2003); Sanchez-Quintana, Anderson and Ho (1996)]. The angles can be adjusted easily for every location when patient-specific fiber orientation data become available. Fig. 3 gives 3D plots of the RV/LV epicardium and endocardium showing fiber orientations matching available patient data. A slice was also given showing our two-layer model structures.

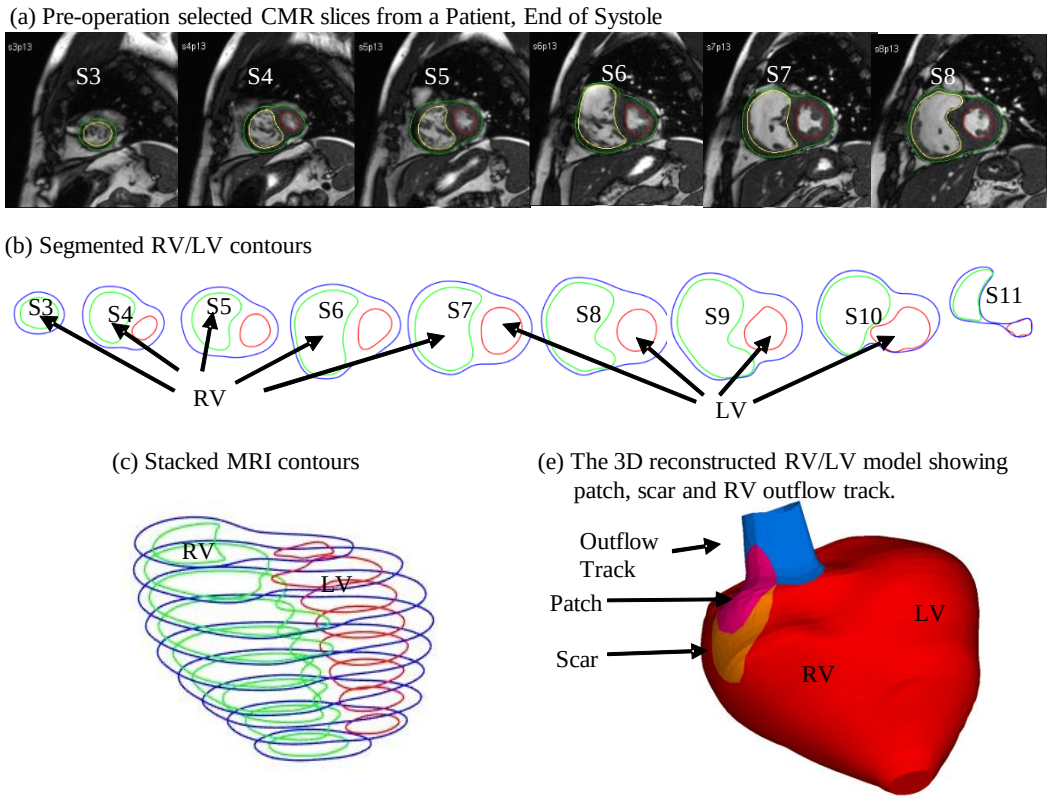


**Figure 2:** Selected MRI slices, segmented slice contour plots, stacked contour 3D view, and 3D plots showing patch, scar and pulmonary outflow track. (a) Selected pre-operation CMR slices from a patient, end of systole; (b) Segmented RV/LV contours; (c) Stacked MRI contours; (d) The final model showing patch, scar and outflow track

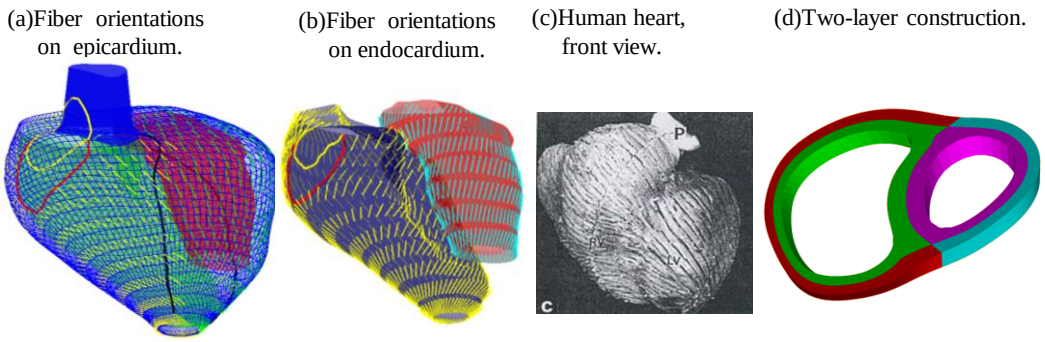


**Figure 3:** Myocardium fiber orientation and two-layer model construction. (a)-(b) Fiber orientation on epicardium and endocardium from our model; (c) A human heart showing fiber orientation [Sanchez-Quintana, Anderson and Ho (1996)]; (d) Two-layer model construction

### *2.2 Geometry-fitting mesh generation technique*

The irregular geometries of human ventricles and patch and scar tissue component inclusions make a geometry-fitting mesh generation technique necessary, which was developed to generate mesh for our RV/LV/Patch/Scar combination models. Considering the two-layer structure and patch and scar component, each slice was first divided into geometry-fitting areas (called "surfaces" in ADINA). The neighboring slices were stacked to form volumes. In this way the 3D RV/LV domain was divided into many small hexahedrons or pentahedrons (called "volumes") to curve-fit the complex RV/LV geometry containing patch and scar. At the same time, each volume has a more regular shape for automatic mesh generation by ADINA. The eventual purpose here is the proper division of each physical object (patch, scar, epicardium and endocardium) into computational volumes so that mesh can be generated. For each volume, we specify mesh density, mesh style and an element group which includes element style, material and other information. Finer mesh was used to the volumes located in the complex structure (RV outlet or pulmonary artery outflow tract). Elements of all the volumes were generated using the ADINA command "Gvolume". For example the pre-op model, M1 contains 1009 small volumes, 28356 nodes and 24762 3D solid elements.

### *2.3 A pre-shrink process to obtain zero-load geometry*

Since a working heart is under constant pressure and its stress/strain conditions are near impossible to measure, we have to start our numerical procedure for the computational models from a no-load geometry with zero pressure and zero stress/strain distributions. A pre-shrink process was used to shrink the in vivo RV/LV geometry to obtain its no-load geometry. The ventricles were then pressurized to recover their in vivo shape with stress/strain calculated. The initial shrinkage for the inner ventricular surface was 2% and pressure was applied to see if the pressurized RV volume matches the CMR data under the minimum pressure. If not, we adjust the shrinkage, re-made the model, pressurize it and check again. The process is repeated until the minimum RV volume of the model under minimum pressure matches CMR volume data with error <0.5%. Ventricle

parameter values were adjusted to match model maximum RV volume under maximal pressure with CMR data. It should be noted that the shrinkage for RV outer wall was smaller than that of RV inner wall so that the RV wall volume (the total tissue vlume, not the chamber) was conserved in the pre-shrink process.

### *2.4 The isotropy and anisotropic structure models*

The governing equations for all material models were:

$$\rho v_{i,tt}=\sigma_{ij,j},\ i,j=1,2,3;\ \text{sum over } j, \tag{1}$$

$$\varepsilon_{ij}=(v_{i,j}+v_{j,i}+v_{\alpha,i}\, v_{\alpha,j})/2, i,j,\alpha=1,2,3, \tag{2}$$

where $\sigma$ is the stress tensor, $\varepsilon$ is the strain tensor, v is displacement, and $\rho$ is material density. The normal stress was assumed to be zero on the outer RV/LV surface and equal to the pressure conditions imposed on the inner RV/LV surfaces. Structure-only RV/LV models were used to optimize model computing time. These models provided RV volume, ejection fractions, and RV stress/strain values for analysis.

The RV and LV materials were assumed to be hyperelastic, anisotropic, nearly-incompressible and homogeneous. The patch and scar materials were assumed to be hyperelastic, isotropic, nearly-incompressible and homogeneous. The nonlinear anisotropic and isotropic Mooney-Rivlin models were used as the material models. The strain energy function for the isotropic modified Mooney-Rivlin model is given by Tang et al. [Tang, Yang, Geva et al. (2008, 2010, 2011)].

$$W=c_1(I_1-3)+c_2(I_2-3)+D_1[\exp(D_2(I_1-3))-1], \tag{3}$$

where $I_1$ and $I_2$ are the first and second strain invariants given by,

$$I_1=\sum C_{ii},\ I_2=\tfrac{1}{2}[I_1^2-C_{ij}C_{ij}], \tag{4}$$

where $C=[C_{ij}]=X^TX$ is the right Cauchy-Green deformation tensor, $X=[X_{ij}]=[\partial x_i/\partial a_j]$, $(x_i)$ is the current position, $(a_i)$ is the original position, $c_i$ and $D_i$ are material parameters chosen to match experimental measurements. The strain energy function for the anisotropic modified Mooney-Rivlin model was obtained by adding an additional anisotropic term in Eq. (4) [Tang, Yang, Geva et al. (2008, 2011)]:

$$W=c_1(I_1-3)+c_2(I_2-3)+D_1[\exp(D_2(I_1-3))-1]+(K_1/K_2)[\exp(K_2(I_4-1)^2)-1], \tag{5}$$

where $I_4=C_{ij}\ (\mathbf{n}_f)_i\ (\mathbf{n}_f)_j$, $C_{ij}$ is the Cauchy-Green deformation tensor, $\mathbf{n}_f$ is the fiber direction, $K_1$ and $K_2$ are material constants. With parameters properly chosen, it was shown that stress-strain curves derived from Eq. (5) agreed very well with the stress-strain curves from the anisotropic (transversely isotropic) strain-energy function with respect to the local fiber direction given in McCulloch et al. [McCulloch, Waldman, Rogers et al. (1992)].

$$W=\frac{C}{2}(e^Q-1), \tag{6}$$

$$Q=b_1E_{ff}^2+b_2(E_{cc}^2+E_{rr}^2+E_{cr}^2+E_{rc}^2)+b_3(E_{fc}^2+E_{cf}^2+E_{fr}^2+E_{rf}^2), \tag{7}$$

where $E_{ff}$ is fiber strain, $E_{cc}$ is cross-fiber in-plane strain, $E_{rr}$ is radial strain, and $E_{cr}$, $E_{fr}$

*and* $E_{fc}$ are the shear components in their respective coordinate planes, $C$, $b_1$, $b_2$, and $b_3$ are parameters to be chosen to fit experimental data. Parameter values in (5)-(7) still needed to be adjusted to fit CMR-measured RV volume data during the pre-shrink process mentioned in Section 2.2. Parameter values in the Mooney-Rivlin models for all materials are summarized in Tab. 1. $c_2$ was set to zero in all models (Fig. 4). Fig. 4 also give the adjusted patient-specific material stress-stretch curves from Mooney-Rivlin models for ventricle tissue, scar and patch materials.

**Table 1:** Summary of parameter values in the modified Mooney-Rivlin models for patch, scar and ventricle materials

| Material/Model | $c_1$ (kPa) | $D_1$(kPa) | $D_2$ | $K_1$(kPa) | $K_2$ |
|---|---|---|---|---|---|
| RV/LV Inner Layer (anisotropic) | 2.43 | 0.77 | 3 | 11.6 | 3 |
| RV/LV Outer Layer (anisotropic) | 2.77 | 0.77 | 3.2 | 11.3 | 3.2 |
| PATCH (isotropic) | 38.5 | 38.5 | 9 | | |
| SCAR (isotropic) | 19.2 | 19.2 | 9 | | |
| Pulmonary Outflow Track (isotropic) | 36.8 | 14.4 | 2 | | |

(a)RV pressure condition in one cardiac cycle

(b) Stress-stretch curves for patch, scar, and ventricular tissue.

(c) Model RV Volume matched CMR RV volume Data.

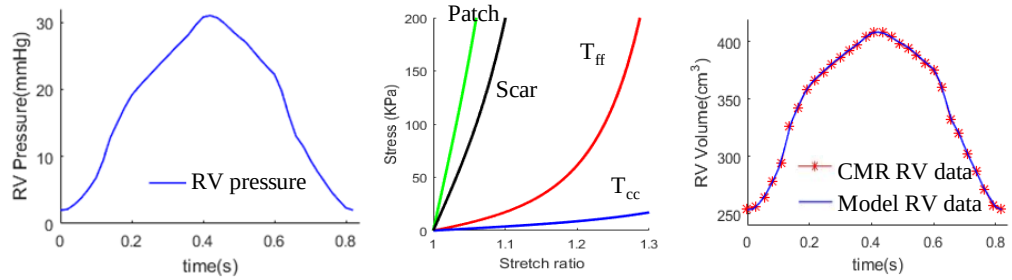


**Figure 4:** Imposed ventricle pressure condition and RV/patch/scar material stress/stretch curves with RV material parameters selected to match CMR-measured volume data. (a) Imposed RV pressure condition; (b) Stress-stretch curves for ventricular tissue and patch/scar materials; (c) Model predicted RV Volume matched CMR RV volume Data

### *2.5 Virtual surgery procedures*

With guidance from cardiac surgeon Dr. del Nido and cardiac radiologist Dr. Geva, we constructed 7 models based on patient-specific CMR RV/LV data as incremental parametric virtual PVR surgery design to evaluate effect of scar trimming and patch size on post-PVR cardiac functions. Three factors were considered: RV remodeling and scar trimming, patch size reduction and myocardium tissue regeneration (replacing patch and scar by normal tissue). The 7 models are: a) Model 1 (M1) which was based on

pre-operative CMR data with the old patch and scar tissues. CMR data for the entire cardiac cycle was used to determine RV tissue material parameter values which were also used in other models (since all models are for the same RV with different surgical options). b) Model 2 (M2) which includes a conventional large patch with some scar trimming. RV volume reduction is about 9%. M2 serves as the baseline model. c) Model 3 (M3) which has the same geometry and patch as M2, but the scar is replaced by normal myocardial tissue (assuming myocardium regeneration would be successful and viable tissue could be generated to replace the scar). d) Model 4 (M4) which has a small patch with aggressive scar trimming and RV remodeling, but still has some residual scar. RV volume reduction is 17%. e) Model 5 (M5) which replaces the residual scar in M4 by regular myocardial tissue; f) Model 6 (M6) which simulates a complete scar trimming procedure (RV shrinkage 25%). RV long axis was reduced as well (see Tab. 2). g) Model 7 (M7) which is the same as M6 except that the patch material is replaced by regular myocardial tissue. A hypothetic ideal tissue engineering method is assumed to make a patch with its mechanical properties similar to contracting myocardium tissue. Tab. 2 provides a summary of the models with their main features. Fig. 5 gives an illustration of the model geometries and different virtual surgery features. All the 7 models were solved and results were obtained for comparison and analysis.

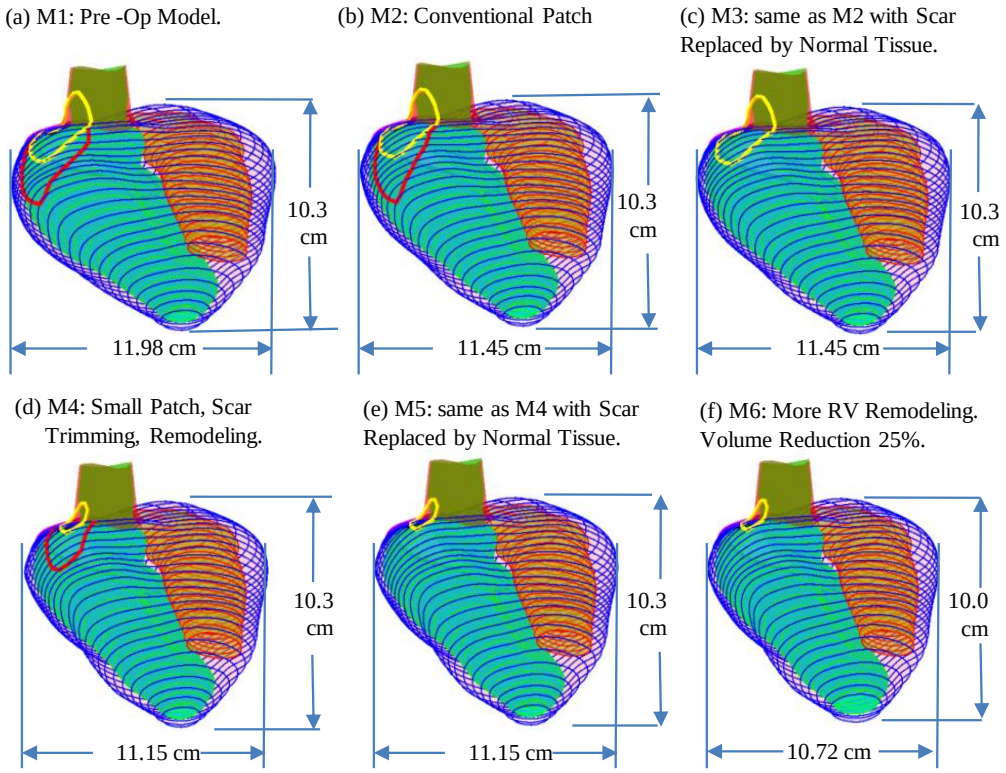


**Figure 5:** Illustration of the virtual surgery models showing key surgical design variations

**Table 2:** Models used for surgical design and optimization

| | |
|---|---|
| M1 | Based on the pre-operation CMR images; Old patch with scar tissue. |
| M2 (baseline) | Conventional patch with scar tissue; A small volume shrinkage 9%. |
| M3 | The same geometry with M2; the scar is replaced of myocardial tissue; Volume shrinkage 9%. |
| M4 | Small patch with aggressive trimming; RV remodeling and scar tissue trimming; RV volume shrinkage 17%. |
| M5 | The same geometry with M4; The residual scar is replaced of myocardial tissue. RV volume shrinkage 17%. |
| M6 | RV shrinkage 25%; No scar. Decrease the height of the model. |
| M7 | The same geometry with M6; The patch will be replaced of myocardial tissue. |

### *2.6 Parameter data extraction and statistical methods*

The 7 models were solved by ADINA and mechanical and geometric parameter values were obtained from the model solutions for analysis and comparison. Surgical option variations included patch size, scar trimming, RV remodeling, and tissue regeneration (assuming availability of tissue). The parameters and quantities used included RV ejection fraction, mean maximum principal stress (Stress-$P_1$), mean maximum principal strain (Strain-$P_1$), mean circumferential curvature (C-cur), and mean RV longitudinal curvature. The two common measures of RV cardiac functions are stroke volume and ejection fraction which are defined as:

SV=RV End Diastolic Volume (RVEDV)–RV End Systolic Volume (RVESV); (8)

EF=[RVEDV - RVESV]/RVEDV. (9)

Mean right ventricle maximum principal stress/strain (mean RV Stress-$P_1$/Strain-$P_1$) were obtained by taking averages of Stress-$P_1$/Strain-$P_1$ values over all computational data points on the RV internal surface, 100 points per slice. Because patch size and material are considered in different virtual surgeries, stress and strain behaviors on the patch edge were also investigated. Circumferential curvature ($\kappa_c$, C-cur) at each point on an RV inner contour was calculated using:

$$\kappa_c = \frac{x'y'' - x''y'}{(x'^2 + y'^2)^{3/2}}, \quad (10)$$

where the contour was treated as a planar curve X=(x(t), y(t)). The derivatives were evaluated using neighboring points on the contour. The formulas used for calculation of longitudinal curvature ($\kappa$, L-cur) at each point was

$$\kappa = \frac{\sqrt{(z''(t)y'(t) - y''(t)z'(t))^2 + (x''(t)z'(t) - z''(t)x'(t))^2 + (y''(t)x'(t) - x''(t)y'(t))^2}}{(x'^2(t) + y'^2(t) + z'^2(t))^{3/2}} \quad (11)$$

where the longitudinal curve (X) was given by X=(x(t), y(t), z(t)) and the derivatives were evaluated with the closest points from neighboring slices vertically below and above the point being considered. One-sided formulas were used for the top and bottom slices.

Outlet/inlet were not taken into the C-cur or L-cur calculation progress.

## 3 Results

The two common measures of RV function evaluated were stroke volume and ejection fraction defined by Eqs. (8)-(9). RV stroke volume and ejection fraction data from the 7 models are given in Tab. 3. Stress-$P_1$, Strain $P_1$, C-cur and L-cur are given in Tab. 4 as an overview of the results. Detailed comparisons and analyses are given in the sub-sections below.

**Table 3:** Stroke volume and ejection fraction comparisons for 7 models showing the model 7 has the best ejection fraction

| | RV Volume No load (ml) | RV Min Volume (ml) | RV Max Volume (ml) | SV (ml) | EF |
|---|---|---|---|---|---|
| Original CMR Data | | 254.79 | 408.76 | 153.97 | 0.3767 |
| M1: Pre-op | 240.04 | 253.79 | 408.62 | 154.83 | 0.3789 |
| M2: Large Patch, Baseline 9% Vol Reduction | 218.63 | 230.95 | 365.98 | 135.03 | 0.3690 |
| M3: Large Patch, 9% Vol Reduction, Scar Replaced by Tissue | 218.63 | 231.14 | 370.12 | 151.48 | 0.3755 |
| M4: Small Patch, Remodeling 17% Vol Reduction | 198.68 | 210.30 | 338.52 | 128.21 | 0.3787 |
| M5: Small Patch, Remodeling, 17% Vol Reduction, Scar Replaced by Tissue | 198.68 | 210.48 | 341.31 | 131.55 | 0.3833 |
| M6: Small Patch, Remodeling, 25% Vol Reduction, Scar Replaced by Tissue. | 179.93 | 190.20 | 308.88 | 118.68 | 0.3842 |
| M7: The deal case 25% Vol Reduction, Patch Replaced by Tissue. | 179.93 | 193.80 | 315.88 | 122.08 | 0.3865 |

### *3.1 Smaller patch led to modestly improved RV post-surgery cardiac function*

Comparing M4 (small patch) with M2 (large patch), EF from M4 was 37.87% while EF from M2 was 36.90%. That is a 2.6% improvement (using 36.9% as base). Mean RV stress from M4 was 43.9 kPa, 0.5% lower than that from M2 (44.1 kPa). Circumferential curvature from M4 was 0.4550 $cm^{-1}$, larger than that from M2 (0.4467 $cm^{-1}$). Longitudinal curvature from M4 was 0.6216 $cm^{-1}$, smaller than that from M2 (0.6606 $cm^{-1}$).

Comparing M5 (small patch with scar replaced by regenerated tissue) with M3 (large

patch but with scar replaced by regenerated tissue), the situation was similar. EF from M5 was 38.33% while EF from M3 was 37.55%. That is a 2% improvement (using 37.55% as base). Mean RV stress from M5 was 42.90 kPa, 2.8% lower than that from M3 (44.10 kPa). Circumferential curvature from M5 was 0.4544 $cm^{-1}$, larger than that from M3 (0.4466 $cm^{-1}$). Longitudinal curvature from M5 was 0.6133 $cm^{-1}$, smaller than that from M3 (0.6482 $cm^{-1}$).

**Table 4:** Summary of RV stress, strain, circumferential curvature and longitudinal curvature from the calculation results of 7 models. All data are mean values of the parameters on RV inner surface data points

| | **Ejection Fraction** | **EF Improve-ment over M2** | **Strain $P_1$** | **Stress $P_1$ (kPa)** | **C-cur ($cm^{-1}$)** | **L- cur ($cm^{-1}$)** |
|---|---|---|---|---|---|---|
| M1: Pre-op, Baseline | 0.3789 | | 0.3268 | 48.03 | 0.4387 | 0.6388 |
| M2: Large Patch, 9% Vol Reduction | 0.3690 | Baseline | 0.3258 | 44.08 | 0.4467 | 0.6606 |
| M3: Large Patch, 9% Vol Reduction, Scar Replaced by Tissue | 0.3755 | 1.76% | 0.3455 | 44.10 | 0.4466 | 0.6482 |
| M4: Small Patch, Remodeling 17% Vol Reduction | 0.3787 | 2.62% | 0.3404 | 43.90 | 0.4550 | 0.6216 |
| M5: Small Patch, Remodeling, 17% Vol Reduction, Scar Replaced by Tissue | 0.3833 | 3.88% | 0.3541 | 42.90 | 0.4544 | 0.6133 |
| M6: Small Patch, Remodeling, 25% Vol Reduction, | 0.3842 | 4.12% | 0.3522 | 41.97 | 0.4572 | 0.6425 |
| M7: Small Patch, Remodeling, 25% Vol Reduction, Patch Replaced by Tissue. | 0.3865 | 4.74% | 0.3546 | 41.88 | 0.4569 | 0.6386 |

### *3.2 Combining small patch and more aggressive RV remodeling led to more improvement on post-surgery cardiac function*

Comparisons of M4 *vs.* M2 and M5 *vs.* M3 already showed that small RV remodeling linked to use of a small patch could lead to modest post-surgery RV cardiac function improvement. M6 utilized more RV remodeling with 25% volume reduction. Tab. 4

showed that EF from M6 was 38.42% while EF from M2 was 36.9%. That is a 4.1% improvement (using 36.9% as base). Mean RV stress from M6 was 41.97 kPa, 4.8% lower than that from M2 (44.08 kPa). Circumferential curvature from M6 was 0.4572 $cm^{-1}$, larger than that from M2 (0.4467 $cm^{-1}$). Longitudinal curvature from M6 was 0.6425 $cm^{-1}$, smaller than that from M2 (0.6606 $cm^{-1}$).

### *3.3 Tissue regeneration technique could have modest improvement on post-surgery cardiac function*

One ideal treatment for myocardium infarction would be tissue regeneration where viable contracting tissue could be regenerated in the infarcted and/or scar areas to bring the heart back to its normal function. Researchers have made considerable effort with encouraging progresses [Skobel, Schuh, Schwarz et al. (2004); Miyahara, Nagaya, Kataoka et al. (2006)]. In our case, assuming contracting ventricle tissue could be made available, we replaced the scar tissue in M3, M5 and M6 to see if that would improve RV cardiac function. Tab. 4 showed that EF from M3 was 37.55% while EF from M2 was 36.9%. That is a 1.8% improvement (using 36.9% as base). Mean RV stress from M3 was 42.10 kPa, which is about the same as that from M2 (44.07 kPa). Longitudinal curvature from M3 was 0.6482 $cm^{-1}$, smaller than that from M2 (0.6606 $cm^{-1}$).

The comparison between M5 and M4 yielded similar results. EF from M5 was 38.33% while EF from M4 was 37.87%. That is a 1.2% improvement (using 37.87% as base). The improvement is smaller because the scar is smaller. Mean RV stresses from M4 and M5 were again about the same. Longitudinal curvature from M5 was 0.6133 $cm^{-1}$, smaller than that from M4 (0.6216 $cm^{-1}$). Tissue regeneration had very little influence in C-cur results.

### *3.4 Combination of multiple surgical techniques led to best improvement on RV post-PVR cardiac function*

More aggressive scar trimming and RV remodeling (25% RV volume reduction) were applied in M6 and M7. M6 has small patch and 25% RV volume reduction. M7 combined all three techniques: small patch, 25% RV volume reduction, and regenerated tissue to replace the patch. The EF from M6 was 38.42% while EF from M2 was 36.9%. That is a 4.1% improvement (using 36.9% as base). Mean RV stresses from M6 was 41.97 kPa, which is 4.8% lower than that from M2.

EF from M7 was 38.65% which was a 4.74% improvement over that from M2 (36.90% as baseline). Mean RV stresses from M7 was 41.88 kPa, which is 5% lower than that from M2 (44.08 kPa). Longitudinal curvature from M7 was 0.6386 $cm^{-1}$, 3.3% smaller than that from M2 (0.6606 $cm^{-1}$). Circumferential curvature from M7 was 0.4569 $cm^{-1}$, 2.28% larger than that from M2 (0.4467 $cm^{-1}$).

### *3.5 Impact of different surgical options on local stress and strain conditions*

From the mechanical point of view, lower stress level means that the ventricle is not working as hard and the surgical repair would last longer (the TOF patients need to do PVR after certain time due to valve failure or other adverse development). However,

patch/scar is only a small portion of the whole RV and comparison of whole RV mean stress values may not show model differences clearly. It is of interest to find out the local stress/strain behaviors in the patch area for model comparisons. Fig. 6 shows the mean values of Stress-$P_1$ and Strain-$P_1$ of the nodes on the edge of patch over a cardiac cycle for the 7 models. Peak stress/strain values in a cardiac cycle for the 7 models were recorded in Tab. 5. Peak Stress-$P_1$ of the patch edge from M7 was 54.26 kPa which is a 30.04% lower than that from M2 (77.56 kPa). Peak Strain-$P_1$ of the patch edge nodes from M7 is 0.2119, which is 171.32% higher than that (0.0781) from M2.

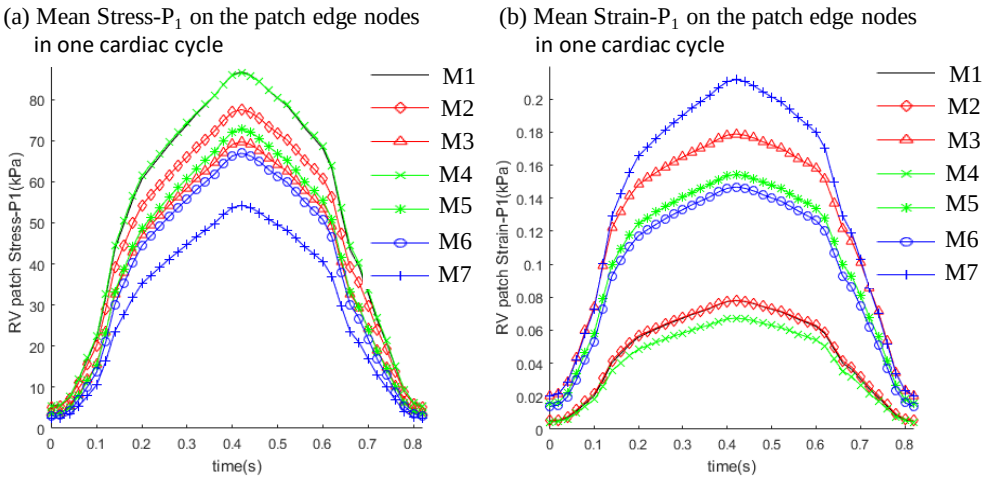


**Figure 6:** RV inner wall stress and strain on the edge of patch

**Table 5:** Summary of peak values of Stress-$P_1$/ Strain-$P_1$ curves on the patch edge from the seven models

| | M1 | M2 | M3 | M4 | M5 | M6 | M7 |
|---|---|---|---|---|---|---|---|
| Stress-$P_1$(kPa) | 86.71 | 77.56 | 69.74 | 86.51 | 72.76 | 66.93 | 54.26 |
| Strain-$P_1$ | 0.0779 | 0.0781 | 0.1789 | 0.0673 | 0.1544 | 0.1467 | 0.2119 |

## 4 Discussion

With the rapidly increasing number of late survivors of Tetralogy of Fallot repair, surgical management of patients with right ventricular dysfunction has become a major clinical challenge. The wide variability in clinical status, extent of right ventricular dilatation, scarring, and dysfunction at the time of presentation has resulted in disparate surgical results with pulmonary valve insertion alone [Waien, Liu, Ross et al. (1992)]. Del Nido and Geva et al. have proposed aggressive scar tissue trimming and RV volume remodeling as a way to improve RV function after pulmonary valve replacement surgery [del Nido (2006)]. A tissue engineering procedure with transplantation of stem cells is expected to repair the scarred and improve ventricular function [Skobel, Schuh, Schwarz et al. (2004); Miyahara, Nagaya, Kataoka et al. (2006)]. In this paper, based on CMR

image and RV pressure data from one patient, 7 RV/LV/Patch/Scar combination models were constructed to investigate impact of different PVR surgical techniques on post-PVR RV cardiac functions. Two patch size, three degrees of scar trimming (RV volume shrinkages: 9%, 17%, 25%) and hypothetical use of regenerated myocardium as replacement of patch and scar were considered in these models. Results presented in this paper indicate that each of the three techniques may have modest improvement on post-PVR RV functions (from 1.76%-4% over M2, the conventional PVR procedure) and combination of all three techniques (M7) had the best performance (a 4.74% improvement over M2). This very limited study also provided some initial evidence that computational simulations may be used to supplement/replace empirical and often risky clinical experimentation, or even guide the design of new clinical trials to examine the efficiency and suitability of various reconstructive procedures in diseased hearts.

Our previous studies (n=10) indicated that mean longitudinal curvature (L-cur) from better-outcome group was 36.5% higher than that from the worse-outcome group [Tang, Yang, Geva et al. (2014)]. Results from this study actually showed that longitudinal curvature (L-cur) was linked to how volume reduction was made: short-axis shortening led to reduction of L-cur (M4 and M5), while long-axis shortening led to increase of L-cur (M6 and M7). No conclusion could be drawn from this single-patient modeling study.

Several improvements can be added to our models in the future for better accuracy and applicability: a) FSI model. FSI models world give flow velocity and fluid shear stress data for more complete analyses. b) Valve mechanics. Valves can be added into our models for better flow control at the inlet and outlet. c) Active contraction model. One way to add active contraction into our model is to introduce an external force field which is tied to fiber structure and orientations. Measurement and validation of the external force field are not currently available. Another way to induce contraction is to make the RV material stiffer during systole. These improvements will be our future directions, each will take considerable effort to implement. Compared with these improved models, we still expect that the SV and EF predictions by our model will have similar accuracies since calculation of SV and EF involves RV volumes and the improved models will also be adjusted to match CMR-measured data. d) More geometric parameters. Some ventricle geometric parameters analyzed in [Tang, Yang, Geva et al. (2017)], such as longitudinal curvature (L-cur), wall thickness (WT) and RV may have correlations with surgical outcome.

It should be noted that the proposed surgical procedure requires long-term efforts from multi-disciplines to get close to and be implemented in clinical practice. The computational simulations (virtual surgery) provided “proof of concept” for further investigations using in vitro experiments, animal models and final patient studies.

## 5 Conclusion

RV/LV/Patch/Scar combination model can be used as a tool for surgical planning and mechanical analysis for ventricular remodeling and tissue regeneration investigations. Our preliminary results indicate that each of the three techniques (smaller patch, RV remodeling, and myocardium regeneration) may have modest improvement on post-PVR RV functions (from 1.76%-4% over the conventional PVR procedure) and combination of all three techniques Could have the best performance (a 4.74% improvement over the current

conventional PVR, for the patient studied). Changes in RV stress, strain and curvature were also observed. However, their linkage to RV function requies further investigations.

**Acknowledgement:** This research was supported in part by NIH grants R01 HL089269 (PI del Nido, Tang, Geva), R01 HL63095 (PI del Nido) and 5P50HL074734 (PI: Geva). Tang's research was also supported in part by National Sciences Foundation of China grants 11672001, 81571691.

**References**

**Axel, L.** (2002): Biomechanical dynamics of the heart with MRI. *Annual Review of Biomedical Engineering*, vol. 4, pp. 321-347.

**del Nido, P. J.** (2006): Surgical management of right ventricular dysfunction late after repair of tetralogy of fallot: Right ventricular remodeling surgery. *Seminars in Thoracic and Cardiovascular Surgery. Pediatric Cardiac Surgery Annual*, vol. 9, no. 1, pp. 29.

**Geva, T.; Greil, G. F.; Marshall, A. C.; Landzberg, M.; Powell, A. J.** (2002): Gadolinium-enhanced 3-dimensional magnetic resonance angiography of pulmonary blood supply in patients with complex pulmonary stenosis or atresia comparison with x-ray angiography. *Circulation*, vol. 106, no. 4, pp. 473-478.

**Geva, T.; Powell, A.; Crawford, E.; Chung, T.; Colan, S.** (1998): Evaluation of regional differences in right ventricular systolic function by acoustic quantification echocardiography and cine magnetic resonance imaging. *Circulation*, vol. 98, no. 4, pp. 339-345.

**Geva, T.; Sandweiss, B. M.; Gauvreau, K.; Lock, J. E.; Powell, A. J.** (2004): Factors associated with impaired clinical status in long-term survivors of tetralogy of fallot repair evaluated by magnetic resonance imaging. *Journal of the American College of Cardiology*, vol. 43, no. 6, pp. 1068.

**Ghista, D. N.; Zhong, L.; Chua, L. P.; Ng, E. Y.; Lim, S. T. et al.** (2005): Systolic modeling of the left ventricle as a mechatronic system: determination of myocardial fiber's sarcomere contractile characteristics and new performance indices. *Molecular & Cellular Biomechanics*, vol. 2, no. 4, pp. 217-234.

**Guccione, J. M.; Costa, K. D.; Mcculloch, A. D.** (1995): Finite element stress analysis of left ventricular mechanics in the beating dog heart. *Journal of Biomechanics*, vol. 28, no. 10, pp. 1167.

**Guccione, J. M.; Le, P. G.; de Tombe, P. P.; Hunter, W. C.** (1997): Measurements of active myocardial tension under a wide range of physiological loading conditions. *Journal of Biomechanics*, vol. 30, no. 2, pp. 189-192.

**Guccione, J. M.; McCulloch, A. D.** (1993): Mechanics of active contraction in cardiac muscle: Part i-constitutive relations for fiber stress that describe deactivation. *Journal of Biomechanical Engineering*, vol. 115, no. 1, pp. 72-81.

**Guccione, J. M.; Waldman, L. K.; Mcculloch, A. D.** (1993): Mechanics of active contraction in cardiac muscle: Part ii-cylindrical models of the systolic left ventricle. *Journal of Biomechanical Engineering*, vol. 115, no. 1, pp. 82-90.

**Haber, I.** (2000): *Three-dimensional motion reconstruction and analysis of the right*

*ventricle from planar tagger MRI (Ph.D. Dissertation)*. University of Pennsylvania.

**Hunter, P. J.; Pullan, A. J.; Smaill, B. H.** (2003): Modeling total heart function. *Annual Review of Biomedical Engineering*, vol. 5, no. 1, pp. 147.

**Long, Q.; Merrifield, R.; Xu, X. Y.; Kilner, P.; Firmin, D. N. et al.** (2008): Subject-specific computational simulation of left ventricular flow based on magnetic resonance imaging. *Proceedings of the Institution of Mechanical Engineers Part H, Journal of Engineering in Medicine*, vol. 222, no. 4, pp. 475-485.

**Long, Q.; Merrifield, R.; Yang, G. Z.; Kilner, P. J.; Firmin, D. N. et al.** (2003): The influence of inflow boundary conditions on intra left ventricle flow predictions. *Journal of Biomechanical Engineering*, vol. 125, no. 6, pp. 922-927.

**McCulloch, A.; Waldman, L.; Rogers, J.; Guccione, J.** (1992): Large-scale finite element analysis of the beating heart. *Critical Reviews in Biomedical Engineering*, vol. 20, no. 5-6, pp. 427.

**McCulloch A. M.** (2007): Continuity 6 (a package distributed free by the National Biomedical Computation Resource). www.continuity.ucsd.edu.

**Miyahara, Y.; Nagaya, N.; Kataoka, M.; Yanagawa, B.; Tanaka, K. et al.** (2006): Monolayered mesenchymal stem cells repair scarred myocardium after myocardial infarction. *Nature Medicine*, vol. 12, no. 4, pp. 459-465.

**Saber, N. R.; Gosman, A. D.; Wood, N. B.; Kilner, P. J.; Charrier, C. L. et al.** (2001): Computational flow modeling of the left ventricle based on in vivo, MRI data: Initial experience. *Annals of Biomedical Engineering*, vol. 29, no. 4, pp. 275-283.

**Sanchez-Quintana, D.; Anderson, R. H.; Ho, S. Y.** (1996): Ventricular myoarchitecture in tetralogy of fallot. *Heart*, vol. 76, no. 3, pp. 280-286.

**Skobel, E.; Schuh, A.; Schwarz, E. R.; Liehn, E. A.; Franke, A. et al.** (2004): Transplantation of fetal cardiomyocytes into infarcted rat hearts results in long-term functional improvement. *Tissue Engineering*, vol. 10, no. 5-6, pp. 849.

**Tang, D.; del Nido, P. J.; Yang, C.; Zuo, H.; Huang, X. et al.** (2016): Patient-specific MRI-based right ventricle models using different zero-load diastole and systole geometries for better cardiac stress and strain calculations and pulmonary valve replacement surgical outcome predictions. *PLOS One*, vol. 11, no. 9, pp. e0162986.

**Tang, D.; Yang, C.; Geva, T.; del Nido, P. J.** (2010): Image-based patient-specific ventricle models with fluid-structure interaction for cardiac function assessment and surgical design optimization. *Progress in Pediatric Cardiology*, vol. 30, no. 1-2, pp. 51-62.

**Tang, D.; Yang, C.; Geva, T.; del Nido, P. J.** (2008): Patient-specific MRI-based 3D FSI RV/LV/patch models for pulmonary valve replacement surgery and patch optimization. *Journal of Biomechanical Engineering*, vol. 130, no. 4, pp. 041010.

**Tang, D.; Yang, C.; Geva, T.; del Nido, P. J.** (2007): Two-layer passive/active anisotropic FSI models with fiber orientation: MRI-based patient-specific modeling of right ventricular response to pulmonary valve insertion surgery. *Mol Cell Biomech*, vol. 4, no. 3, pp. 159-176.

**Tang, D.; Yang, C.; Geva, T.; del Nido, P. J.** (2014): Right ventricular local longitudinal curvature as a marker and predictor for pulmonary valve replacement surgery outcome:

An initial study based on preoperative and postoperative cardiac magnetic resonance data from patients with repaired tetralogy of Fallot. *Journal of Thoracic & Cardiovascular Surgery*, vol. 147, no. 1, pp. 537-538.

**Tang, D.; Yang, C.; Geva, T.; Gaudette, G.; del Nido, P. J.** (2011): Multi-physics MRI-based two-layer fluid-structure interaction anisotropic models of human right and left ventricles with different patch materials: cardiac function assessment and mechanical stress analysis. *Computers & Structures*, vol. 89, no. 11-12, pp. 1059-1068.

**Tang, D.; Yang, C.; Geva, T.; Rathod, R. H.; Yamauchi, H. et al.** (2013): A multiphysics modeling approach to develop right ventricle pulmonary valve replacement surgical procedures with a contracting band to improve ventricle ejection fraction. *Computers & Structures*, vol. 122, no. 2, pp. 78-87.

**Tang, D.; Zuo, H.; Wu, Z.; Huang, X.; Rathod, R. H. et al.** (2017): Comparison of right ventricle morphological and mechanical characteristics for healthy and patients with tetralogy of fallot: An in vivo mri-based modeling study. *Molecular & Cellular Biomechanics*, vol. 14, no. 3, pp. 137-151.

**Therrien, J.; Siu, S. C.; Mclaughlin, P. R.; Liu, P. P.; Williams, W. G. et al.** (2000): Pulmonary valve replacement in adults late after repair of tetralogy of fallot: Are we operating too late? *Journal of the American College of Cardiology*, vol. 36, no. 5, pp. 1670-1675.

**Vetter, F. J.; Mcculloch, A. D.** (2000): Three-dimensional stress and strain in passive rabbit left ventricle: A model study. *Annals of Biomedical Engineering*, vol. 28, no. 7, pp. 781-792.

**Vliegen, H. W.; Van, S. A.; De, R. A.; Roest, A. A.; Schoof, P. H. et al.** (2002): Magnetic resonance imaging to assess the hemodynamic effects of pulmonary valve replacement in adults late after repair of tetralogy of fallot. *Circulation*, vol. 106, no. 13, pp. 1703-1707.

**Waien, S. A.; Liu, P. P.; Ross, B. L.; Williams, W. G.; Webb, G. D. et al.** (1992): Serial follow-up of adults with repaired tetralogy of fallot. *Journal of the American College of Cardiology*, vol. 20, no. 2, pp. 295.

**Wenk, J. F.; Zhang, Z.; Cheng, G.; Malhotra, D.; Acevedo-Bolton, G. et al.** (2010): First finite element model of the left ventricle with mitral valve: insights into ischemic mitral regurgitation. *Annals of Thoracic Surgery*, vol. 89, no. 5, pp. 1546-1553.

**Yang, C.; Tang, D.; Geva, T.; Rathod, R.; Yamauchi, H. et al.** (2013): Using contracting band to improve right ventricle ejection fraction for patients with repaired tetralogy of fallot: A modeling study using patient-specific CMR-based 2-layer anisotropic models of human right and left ventricles. *Journal of Thoracic & Cardiovascular Surgery*, vol. 145, no. 1, pp. 1-2.

**Yang, C.; Tang, D.; Haber, I.; Geva, T.; del Nido, P. J.** (2007): In vivo MRI-based 3D FSI RV/LV models for human right ventricle and patch design for potential computer-aided surgery optimization. *Computers & Structures*, vol. 85, no. 11-14, pp. 988-997.